Individual addressing of ion qubits with counterpropagating optical frequency combs

Evgeny Anikin ⬡, Lianna A. Akopyan ⬡, Mikhail Popov ⬡, Yelnury Suleimen ⬡,
Olga Lakhmanskaya ⬡, and Kirill Lakhmanskiy ⬡
Russian Quantum Center, Skolkovo, Moscow 143025, Russia

We propose a method of individual single-qubit addressing of linear trapped-ion chains utilizing two ultrastable femtosecond frequency combs. For that, we suggest implementing the single-qubit gates with two counterpropagating frequency combs overlapping on the target ion and causing the ac Stark shift between the qubit levels. With analytical calculations and numerical modeling, we show that the arbitrary single-qubit rotations can be indeed realized using only laser fields propagating along the ion chain. We analyze the error sources for the proposed addressing method and prove that it allows implementing the single-qubit gates with high fidelity.

I. INTRODUCTION

Trapped-ion quantum computers are one of the most promising platforms for quantum computation [1,2]. Their beneficial features include long qubit coherence times [3,4], high entangling gate fidelities [5,6], and all-to-all qubit connectivity. With trapped-ion quantum computers, highly entangled states have been prepared [7], and quantum circuits consisting of multiple gates have been realized [8,9]. Also, trapped ions allowed performing quantum simulations of various spin models with up to 53 spins [10–13]. However, scaling the trapped ion quantum computers up to more than tens of qubits remains challenging [14].

One of the necessary components to perform quantum operations with trapped ions is individual addressing, meaning the ability to apply the control laser field to an individual ion to perform gate operations. The existing approaches to perform addressing include the usage of microoptics splitting modules [7,15], acoustooptical deflectors [7], multichannel acoustooptical modulators [9], microelectromechanical mirror systems [16], or integrated-optical waveguides [17]. However, the difficulty of the technical realization of these approaches increases with the growing number of ions. Thus, designing new approaches to individual addressing is of great interest to the development of the large-scale quantum computer based on trapped ions. In this paper, we suggest a scalable method of single-qubit addressing in trapped-ion quantum computers utilizing femtosecond frequency combs.

Ultrastable femtosecond frequency combs generated by mode-locked lasers [18] have multiple applications in the field of quantum information processing, in particular, for quantum computing with atomic ions. For example, the remarkable spectral purity of the frequency combs enabled their usage to produce entanglement between two atomic ions via Raman transitions [19]. Also, the high instantaneous field intensity and the short pulse duration allowed the implementation of ultrafast gates [20] and the generation of ultrafast spin-motion entanglement [21].

In trapped-ion quantum computers, the most frequently used ions configuration is a linear chain [2]. We suggest a method to perform individual single-qubit operations in linear chains of optical ion qubits with two ultrastable femtosecond frequency combs with the same repetition rate counter-propagating along the chain. To select the target ion, the delay between the comb pulses should be adjusted to overlap them on the target ion. After the action of the two trains of pulses, the rotation of the target qubit differs from the rotation of the other ones due to the nonlinearity of the ion-field interaction. The beneficial feature of the suggested method is that the setup geometry is independent of the number of ions in the chain.

We demonstrate the feasibility of such an approach for optical ^{40}Ca$^+$ qubits. We consider the interaction of the ^{40}Ca$^+$ qubit with the off-resonant comb field inducing the ac Stark shift [22] on the qubit levels which induces optical qubit Bloch sphere rotations by arbitrary angle about the Z axis. Our calculations show that these gates can be implemented with reasonable gate time and high fidelity. Thus, the suggested method can become an effective tool for quantum operations in the ion chain.

II. ARBITRARY LOCAL GATE BASED ON AC STARK SHIFT

The key idea of our method is to illuminate the ion chain with two frequency combs which propagate along the ion chain in opposite directions [see Fig. 1(a)]. For such geometry, there exist spatial regions where the pulses from different combs overlap. The length of the femtosecond pulse is of the order of the interionic distance, so it is possible to make only one target qubit lie in the overlap region. The action of the field on the ion in the overlap region differs from the one outside of it due to the intrinsic nonlinearity in the ion-field interaction. This allows acting selectively on an arbitrary ion by controlling the time delay between the combs: the time delay should be chosen to overlap the pulses on a target ion.

The nonlinear effect that we utilize is the quadratic ac Stark shift of the qubit levels, which implies a large detuning of the comb frequencies from the ion transition frequencies. Then, the main effect of each comb pulse is the phase accumula-
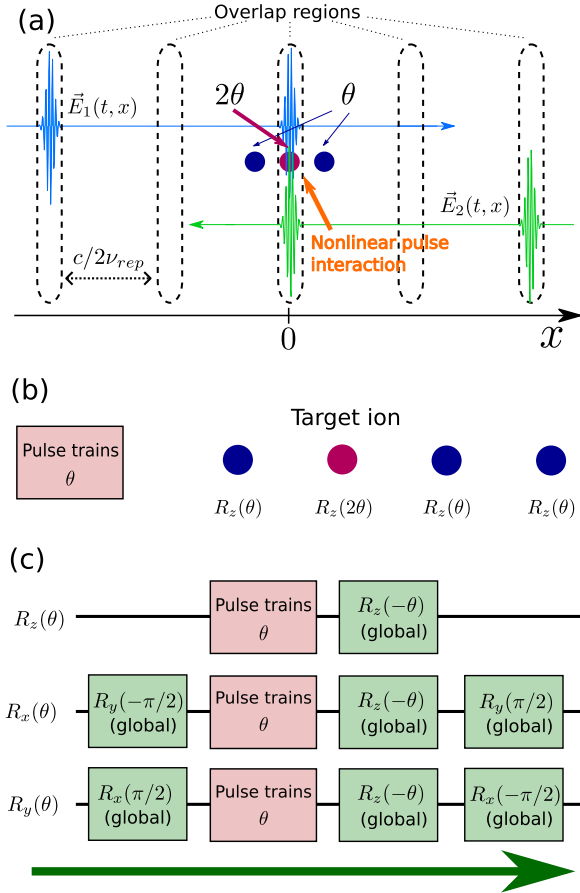
FIG. 1. (a) Ion chain in the linear trap and comb pulses propagating along it (x axis). Comb pulses overlap on the target ion. (b) The phases acquired by the ion chain after the action of two counterpropagating pulse trains. (c) The implementation of the local $R_x(\theta)$, $R_y(\theta)$, $R_z(\theta)$ operations on a target ion. The arrow represents the order in which the operators should be performed (from left to right).

tion on each of the ion levels, in particular, on qubit levels. Therefore, the action of the comb reduces to the $R_z(\theta)$ gate for each qubit. Here $R_x(\theta)$, $R_y(\theta)$, $R_z(\theta)$ denote qubit Bloch sphere rotations by angle θ about the corresponding axes.

At the position of the target ion, the pulses form an interference pattern. The electric field in the largest interference peak is twice the maximum of the field magnitude of a single pulse. The electric field of the combs induces the phase shifts between the ion qubit levels due to the ac Stark effect. As the ac Stark effect is quadratic in the field amplitude, the phase shift is four times larger than the phase shift from a single pulse.

Therefore, the cumulative effect of the two trains of N_{pulses} pulses on the ion qubit levels $|0\rangle$ and $|1\rangle$ is an $R_z(\theta)$ rotation. The rotation angle is $2\theta = 4N_{\text{pulses}}(\delta\theta_1 - \delta\theta_0)$ for the target ion and $\theta = 2N_{\text{pulses}}(\delta\theta_1 - \delta\theta_0)$ for nontarget ions [see Fig. 1(b)], where $\delta\theta_{0,1}$ are the acquired phases per single comb pulse for the levels 0 and 1, respectively. To apply the $R_z(\theta)$ rotation only on the target ion, the pulse trains need to be followed by a global $R_z(-\theta)$ rotation. Further, local $R_x(\theta)$ and $R_y(\theta)$ rotations can be implemented with the help of additional

global $\pm\pi/2$ rotations before and after the pulse train [see Fig. 1(c)] [23].

The choice of the comb wavelength is justified by two requirements. First, the combs should be detuned far enough from the transitions between the qubit levels and the short-living $4P_{1/2}$ and $4P_{3/2}$ levels, otherwise, photon scattering will lead to large qubit decoherence. As the spectral width of femtosecond pulses is a tenth of terahertz, the detunings should be at least the same order or larger. Second, the comb wavelength should be far enough from the magic wavelength of qubit transitions [24], which ensures that the phase acquired by the qubit is sufficiently large. For the $^{40}\text{Ca}^+$, both of these requirements are satisfied for the 1000-nm frequency comb.

The comb repetition rate ν_{rep} should be chosen so that the distance $c/2\nu_{\text{rep}}$ between the overlap regions is larger than the ion chain length. This ensures that only one overlap region is present within the chain (see Fig. 1). As the typical length of long ion chains is hundreds of μm [12], the upper limit on ν_{rep} is hundreds of GHz.

The theoretical analysis of the subsequent sections shows that for the $^{40}\text{Ca}^+$ ion, the $\sim$1000-nm frequency combs with a pulse duration of 20 fs and a repetition rate of 100 MHz allow implementing the single-qubit $R_z(\pi/2)$ rotations with the infidelity of $\sim$5 × 10^{-4} and the gate duration of $\sim$8 μs.

III. THEORETICAL DESCRIPTION OF THE GATE IMPLEMENTATION

To find parameters for the suggested gate implementation, we derive the evolution operator for trapped ions interacting with the electromagnetic (EM) field $\vec{E}(t, \hat{x})$ of the combs using the following Hamiltonian:

$$\mathcal{H} = \hat{H}_0 - \vec{E}(t, \hat{x})\hat{\vec{d}} + \sum_\lambda \hbar\omega_\lambda \hat{a}_\lambda^\dagger \hat{a}_\lambda,$$

$$\hat{H}_0 = \sum_\alpha \epsilon_\alpha |\alpha\rangle\langle\alpha|, \quad \hat{\vec{d}} = \sum_{\alpha\beta} \vec{d}_{\alpha\beta} |\alpha\rangle\langle\beta|,$$

$$\hat{x} = x_0 + \sum_\lambda \frac{\eta_\lambda}{k_c}(\hat{a}_\lambda + \hat{a}_\lambda^\dagger). \quad (1)$$

Here $\hat{H}_0$ is the Hamiltonian of a single ion with the electronic levels α; ϵ_α are their corresponding energies; $\hat{\vec{d}} = (\hat{d}_x, \hat{d}_y, \hat{d}_z)$ is the ion dipole moment operator defined in the basis of the electronic states α, β; η_λ is the Lamb-Dicke parameter of the normal mode λ; $k_c = \omega_c/c$ is the comb wave vector; and $\hat{a}_\lambda^\dagger$, $\hat{a}_\lambda$ are phonon creation and annihilation operators. For the energy-level structure and the dipole-allowed transitions of the $^{40}\text{Ca}^+$ ion, see Fig. 2 (see also [25]).

For our purposes, it is convenient to write the field of two combs $\vec{E}(t, \hat{x})$ acting on each ion in the form where contributions from each comb are grouped into pairs:

$$\vec{E}(t, x) = \sum_{k=1}^{N_{\text{pulses}}} \mathcal{E}_k(t, x)\vec{u}, \quad (2)$$

$$\mathcal{E}_k(t, x) = E_{\text{env}}\left(t - kT - t_1 - \frac{x}{c}\right)e^{-i\omega_c(t-t_1-\frac{x}{c})}$$

$$+ E_{\text{env}}\left(t - kT - t_2 + \frac{x}{c}\right)e^{-i\omega_c(t-t_2+\frac{x}{c})} + \text{c.c.} \quad (3)$$
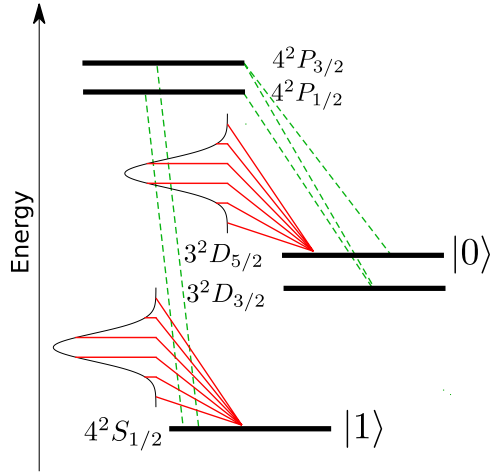
FIG. 2. The energy levels of the $^{40}\text{Ca}^+$ ion (black lines, not to scale) together with the frequency comb spectrum (red lines). The carrier frequency of the comb is far detuned from all the transitions between the ion levels. The green dashed lines represent the dipole allowed transitions.

Here $T = \frac{1}{\nu_{\text{rep}}}$ is the time between the pulses, $t_{1,2}$ are the delay times of the combs, $\vec{u}_{1,2}$ are polarization vectors of the combs, and ω_c is the carrier offset frequency. The envelopes $E_{\text{env}}(t)$ of the comb pulses are smooth functions quickly decaying away from $t = 0$, in particular, we assume Gaussian shape $E_{\text{env}}(t) = E_{\text{peak}} e^{-t^2/\tau^2}$. The terms $\mathcal{E}_k(t, x)$ contain contributions of the kth pulses of both frequency combs. We can separate the contributions of different pairs of pulses because

in our scheme the kth pulses from both combs come with the delay of tens of femtoseconds, whereas the interval between the adjacent pulses is tens of nanoseconds.

We use the following strategy to find the evolution operator of an ion in the field of the frequency combs. We find the evolution operator for each couple of pulses and then multiply all the operators for all couples. The free evolution between the couples is represented by the identity operator, so the evolution operator of the train of pulses reads

$$U_{\text{total}} = U_{N_{\text{pulses}}} U_{N_{\text{pulses}}-1} \ldots U_1, \tag{4}$$

where each operator U_k represents the action of the kth couple of pulses with the field $\mathcal{E}_k$ in the interaction representation.

In the interaction picture, the unitary rotation U_k can be found with the help of the perturbation theory based on Magnus expansion [26]. It is sufficient to consider the Magnus expansion up to the second order as the phase shift on the ion levels appears first in the second order. Thus, the evolution operator in the interaction representation reads

$$U_k = e^{X_k + Y_k}, \tag{5}$$

where X_k and Y_k are the first-order and the second-order contributions of the kth couple of pulses.

Using the Fourier image of the field $\mathcal{E}_k(\omega)$ of the couple of pulses and ignoring the contribution of the phonon modes, we obtain

$$(X_k)_{\alpha\beta} = -i\mathcal{E}_k(\epsilon_\alpha - \epsilon_\beta)(\vec{u}\vec{d})_{\alpha\beta}, \tag{6}$$

$$(Y_k)_{\alpha\beta} = +i \int \frac{d\omega}{2\pi} \mathcal{E}_k\left(\frac{\epsilon_\alpha - \epsilon_\beta}{2} - \omega\right) \mathcal{E}_k\left(\frac{\epsilon_\alpha - \epsilon_\beta}{2} + \omega\right) \sum_\gamma \frac{(\vec{u}\vec{d})_{\alpha\gamma}(\vec{u}\vec{d})_{\gamma\beta}}{\epsilon_\gamma - \frac{\epsilon_\alpha + \epsilon_\beta}{2} - \omega}. \tag{7}$$

Equations (6) and (7) contain all possible contributions from the single-photon and two-photon processes except those involving the phonon modes (for the latter, see Sec. IV). $(X_k)_{\alpha\beta}$ contains contributions from single-photon absorption and stimulated emission and can be neglected since the considered comb fields are off-resonant with atomic transitions. $(Y_k)_{\alpha\beta}$ contains contributions from two-photon transitions, Raman transitions, and photon forward scattering. Among these processes, two-photon absorption and emission can be neglected as they are off-resonant. Raman transitions are pos-

sible and there is a nonzero transition amplitude between the ion fine-structure components, Zeeman sublevels, or oscillatory levels for each couple of pulses. However, for a long train of pulses, these amplitudes interfere destructively unless the transition frequency between the levels is close to an integer multiple of the combs repetition rate (see discussion in Sec. IV and Appendix A). Thus, the only remaining effect is photon forward scattering which leads to the phase accumulated on each ion level. The phases can be directly found from the diagonal components of $Y_{\alpha\beta}$. For the ion at the position x, the acquired phase on the level α is

$$\delta\theta_\alpha(x) = -iY_{\alpha\alpha} \approx 4 \int \frac{d\omega}{2\pi} |E_{\text{env}}(\omega - \omega_c)|^2 \left\{1 + \cos\left[\omega\left(t_1 - t_2 + \frac{2x}{c}\right)\right]\right\} \sum_\gamma \frac{(\epsilon_\gamma - \epsilon_\alpha)|(\vec{u}\vec{d})_{\alpha\gamma}|^2}{(\epsilon_\gamma - \epsilon_\alpha)^2 - \omega^2}, \tag{8}$$

where $E_{\text{env}}(\omega)$ is the Fourier image of a single pulse envelope and only the resonant contributions to the $Y_{\alpha\alpha}$ are kept.

The behavior of the phases $\delta\theta_\alpha(x)$ for the levels of the $^{40}\text{Ca}^+$ is shown in Fig. 3. The phases $\delta\theta_\alpha(x)$ have oscillatory

dependence on x due to the interference of combs. They vanish away from the overlap region and the phases approach the constant value. In the center of the overlap region [at $x = c(t_2 - t_1)/2$], the phases are twice of the value far away from
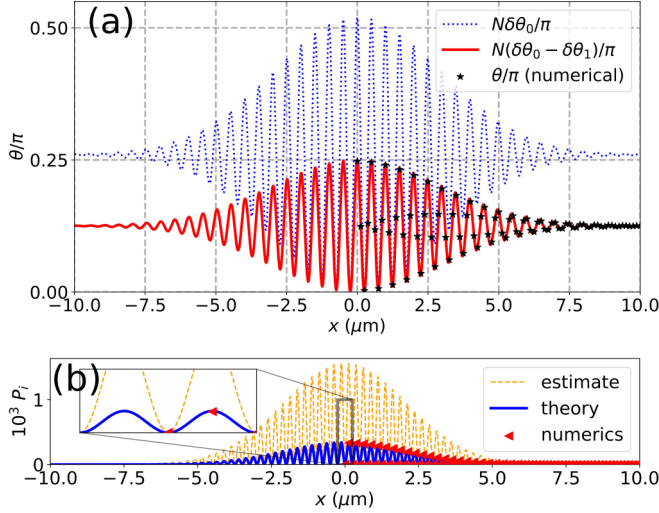
FIG. 3. (a) The phases acquired on the ion qubit levels $|0\rangle = |D_{5/2}, m = -1/2\rangle$ and $|1\rangle = |S_{1/2}, m = -1/2\rangle$ after the action of $N_{\text{pulses}} = 200$ couples of combs pulses depending on the ion coordinate x The parameters of combs are taken from Table I. (b) The probability of the phonon mode excitation for the initial state $|\psi_{\text{init}}\rangle = \frac{1}{\sqrt{2}}(|0\rangle + |1\rangle)$. The orange dashed line represents the upper estimate (11), the blue solid line represents the analytical expression (B5), and red triangles represent the numerically simulated values.

it. Thus, by applying N_{pulses} couples of pulses to the ion chain with the combs delays t_1 and t_2 such as $x_{tg} = c(t_2 - t_1)/2$, one can implement the $R_z(2\theta)$ rotation on the target ion with the coordinate x_{tg} and $R_z(\theta)$ rotation on all other ions, where

$$\theta = N_{\text{pulses}}\delta\theta(x_{tg}) = N_{\text{pulses}}[\delta\theta_1(x_{tg}) - \delta\theta_0(x_{tg})]/2, \quad (9)$$

with the indices 0, 1 denoting the qubit levels and the gate duration of $N_{\text{pulses}}T$.

With Eq. (8), we calculate the phase shifts for the $4S_{1/2}$, $m = -1/2$ and $3D_{5/2}$, $m = -1/2$ levels of the $^{40}\text{Ca}^+$ ion. The energy levels (see Fig. 2) are taken from the NIST database [25], and we calculate the transition dipole moments from the decay rates taken from the NIST database. The parameters of combs are taken from Table I. The field

TABLE I. The parameters chosen for the analysis of single-qubit trapped-ion gates performed with frequency combs.

Combs parameters		
Carrier wavelength	λ_c	1000 nm
Pulse duration	τ	20 fs
Repetition rate	ν_{rep}	100 MHz
Polarization	$\vec{u}$	$(0, 0, 1)^T$
Peak electric field	$ea_0 E_{\text{peak}}/\hbar$	≈ 4.405 THz
Trap parameters		
Axial frequency	$\omega_{ax}/(2\pi)$	600 kHz
Lamb-Dicke parameter	η	0.09
Predicted gate parameters		
Angle per couple of pulses	$\delta\theta(x = 0)$	$\pi/1600$
Qubit rotation speed	$\frac{d\theta}{dt}$	$\pi/16\,\mu\text{s}^{-1}$
Infidelity	$1 - F$	5×10^{-4}

polarization is taken as $\vec{u} = (0, 0, 1)^T$ (parallel to the quantization axis) for simplicity and the value of the electric field is chosen in order to achieve the qubit rotation speed of $\frac{d\theta}{dt} = \pi/16\,\mu\text{s}^{-1}$. This allows performing a $\pi/2$ rotation per $8\,\mu\text{s}$ with 800 combs pulses, which is comparable with the duration of single-qubit gate implemented with continuous-wave lasers.

Also, by the appropriate choice of the comb wavelength and intensity, our method can be adjusted for the $^{88}\text{Sr}^+$, $^{138}\text{Ba}^+$, and $^{226}\text{Ra}^+$ ions which have a similar structure of the energy levels (see Fig. 2).

IV. GATE ERRORS

In this section, we analyze the sources of infidelity for the considered gate implementation, which we list as follows:

(1) Unwanted rotations of the non-target qubits;

(2) Photon scattering;

(3) Transitions between the electronic or vibrational levels;

(4) Fluctuations of the comb field.

The unwanted rotations of the non-target qubits (the crosstalk) occur because the phase shifts of the nontarget qubits are not exactly equal to each other. This leads to the incomplete cancellation of their phases when the global rotations are applied [see Figs. 1(b) and 1(c)]. The dominant contribution to the error comes from the nearest neighbors of the target qubit. Given that the target qubit rotates by 2θ, the neighbor ones rotate by $\theta + \delta\theta$. For the other ions, one can neglect the incomplete phase cancellation due to the rapid decay of the phases oscillations in Eq. (8). Then, the contribution to the gate infidelity can be estimated as $\delta\theta^2$. For the interionic distance of $10\,\mu\text{m}$, we calculate the phase difference $\delta\theta$ with the help of Eq. (8) and find that $\delta\theta \sim 10^{-2}$ for $\theta \sim 1$, which leads to the contribution to the gate infidelity of $\sim 10^{-4}$.

For photon scattering, we estimate its contribution into the gate infidelity as the mean number of scattered photons (both elastically and inelastically) by all ions after the action of the train of pulses. Given that the full scattering cross section of a photon with the frequency ω is $\sigma(\omega)$, we calculate the mean number of photons scattered by a single ion from a single comb pulse $E(t)$ as

$$N_{\text{scattered}} = \frac{\epsilon_0 c}{\hbar} \int_0^\infty \frac{d\omega}{\pi} \frac{\sigma(\omega)}{\omega} |E(\omega)|^2. \quad (10)$$

The cross section $\sigma(\omega)$ is given by the Kramers-Heisenberg formula [27] integrated over the scattered photon angles and summed over all possible final states. In the Kramers-Heisenberg formula, we carefully take into account the finite lifetime of the intermediate $P_{1/2}$ and $P_{3/2}$ levels to avoid singularities in the integral. The resulting probability to emit a photon per pulse at the considered parameters does not exceed 10^{-9}, which leads to the contribution to infidelity of $\sim 10^{-6}$ per ion for ~ 1000 pulses.

Then, we analyze the contribution of the transitions between the electronic and the vibrational levels. We claim that the most important processes contributing to the gate error are the following Raman transitions:

(1) Between different fine structure sublevels: $D_{5/2} \to D_{3/2}$;

(2) Between different Zeeman components of the qubit manifolds;

(3) Between different oscillatory levels (equivalent to the phonon creation and annihilation).

Among the other possible transitions, the excitation of the short-living $P_{1/2}$ and $P_{3/2}$ levels contributes to the photon scattering discussed above, as the excited $P_{1/2}$ and $P_{3/2}$ levels quickly decay with the emission of a photon. Also, the quadrupole and magnetodipole transitions between the S and D levels and the two-photon absorption and emission processes are strongly off-resonant and thus can be neglected.

In contrast, for the processes (a) to (c), the single-pulse transition amplitudes have comparable magnitude with the phase shifts defined by Eq. (8) because of the large spectral width of pulses exceeding even the fine splitting. However, the total pulse train contribution obtained by summation of all pulse amplitudes remains small due to destructive interference between pulses. This happens because the transition amplitude from the ion level α to the level γ induced by the kth pair of pulses contains an oscillating phase factor of $e^{i(\epsilon_\gamma - \epsilon_\alpha)kT}$. The contributions of individual pulses nearly cancel each other for long pulse trains.

The detailed calculations for the processes (a) and (b) are presented in Appendix A. There, we consider a pulse train inducing the rotation by angle $\theta \sim 1$ and find the transition amplitudes by direct summation of all the single-pulse amplitudes. For the transition amplitude $D_{5/2} \to D_{3/2}$, the total transition probability remains as small as $\sim 1/N_{\text{pulses}}^2 \sim 10^{-6}$ providing that the transition frequencies between the qubit $D_{5/2}$ level and $|D_{3/2}, m\rangle$ levels are not the integer multiples of the repetition rate. For the transitions between the Zeeman sublevels of the $D_{5/2}$, we estimate the transition probability as $(\frac{\nu_{\text{rep}}}{2\pi N_{\text{pulses}} \nu_z})^2 \sim 10^{-4}$, where ν_z is the Zeeman splitting.

For process (c), we calculate the probability of the phonon mode excitation with the help of the effective Hamiltonian for the qubit levels and phonon modes (see details in the Appendix B). We derive the effective Hamiltonian using the fact that the normal-mode oscillation period is much larger than the single pulse duration and considerably larger than the period between pulses. Given that the ion is initially in the state $|\psi_{\text{init}}\rangle = c_0|0\rangle + c_1|1\rangle$, the estimate for the phonon excitation probability reads [see Eq. (B5)]

$$P_i = |c_0|^2 P_{i0} + |c_1|^2 P_{i1} < P_{i0}, \quad P_{i\alpha} < \frac{c^2}{\omega_c^2}\left(\frac{\partial \delta\theta_\alpha}{\partial x}\right)^2 \sum_\lambda \frac{4|\eta_{i\lambda}|^2}{\omega_\lambda^2 T^2},$$

(11)

where i is the ion number, λ enumerates the axial phonon modes, and $\eta_{i\lambda}$ are the Lamb-Dicke parameters. The first inequality holds because $P_{i0} > P_{i1}$.

According to Eq. (11), the phonon excitation probability vanishes when the ion is in the center of the interference peak. However, it may significantly contribute to the error in a realistic setup if the center of the interference peak deviates from the ion position. To estimate the phonon excitation probability, we assumed the deviation of 30 nm. For a single ion characterized by parameters of Table I, we use Eq. (11) to prove that the phonon excitation probability does not exceed 3×10^{-4} [see Fig. 3(b)]. For longer ion chains, we find that a similar level of phonon excitation error can be achieved
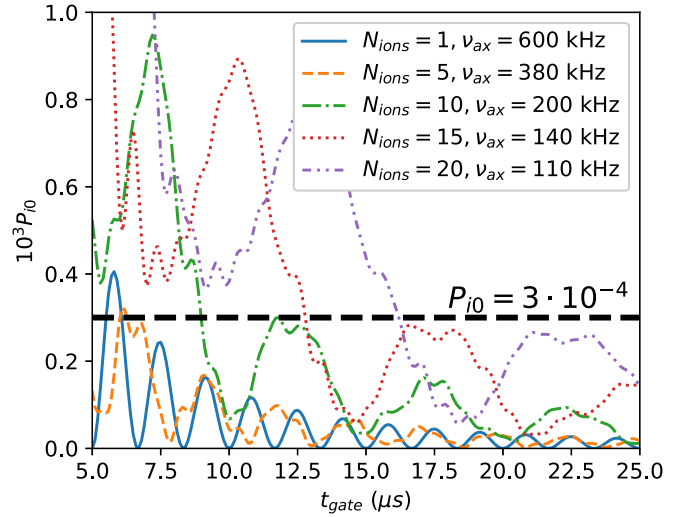

FIG. 4. The probability of the phonon excitation for a center ion of the chain with N_{ions} ions in $|0\rangle$ state depending on gate duration at the rotation angle of $\pi/2$. The horizontal dashed line indicates the probability level of 3×10^{-4}.

with the appropriate choice of gate duration (see Appendix B, Fig. 4).

Finally, let us discuss the effect of comb field fluctuations. We assume that the pulse trains coming from both sides originate from a single frequency comb source. Then, phase fluctuations of the comb source and the fluctuations of the pulse shape do not affect the interference pattern for the intensity in the pulses overlap region and therefore the gate performance. Thus, the main effect comes from overall intensity fluctuations, which can be estimated the same way as for continuous wave lasers. For continuous wave lasers, the contribution of intensity fluctuations into infidelity is typically of order $\sim 10^{-4}$ [5] and can be further reduced with intensity stabilization techniques [28]. Therefore, we do not include this type of error in our error budget.

All the discussed errors (except for comb field fluctuations) are presented in Table II. The dominant contributions are the crosstalk, transitions to Zeeman sublevels and phonon excitation error. We estimate the total contribution for the suggested parameters as 5×10^{-4}.

V. NUMERICAL MODELING

We verify the theoretical considerations of Secs. III and IV with the numerical simulation of the $^{40}\text{Ca}^+$ ion in the field of

TABLE II. The contributions to the frequency-comb based gate error discussed in Sec. IV.

Error source	Contribution
Crosstalk	10^{-4}
Photon scattering	10^{-5}
Transitions to nonqubit Zeeman sublevels	10^{-4}
Transitions to $D_{3/2}$ sublevels	10^{-6}
Phonon excitation	3×10^{-4}
Total error	5×10^{-4}

two counterpropagating frequency combs. In the simulation, we consider the low-lying S, P, and D levels of the ^{40}Ca$^+$ ion, the interaction of the internal degrees of freedom of the ion with one vibrational mode of the ion chain and radiative decay of the short-living P levels.

For the verification, we simulate the quantum dynamics of the ion using the master equation in the Lindblad form [29,30]

$$\frac{d\hat{\rho}}{dt} = -\frac{i}{\hbar}[\hat{\mathcal{H}}, \hat{\rho}] + \mathcal{L}\hat{\rho}, \tag{12}$$

where $\hat{\rho}$ is the density matrix of the ion-phonon system, $\hat{\mathcal{H}}$ is the Hamiltonian (1), and $\mathcal{L}$ is a spontaneous relaxation superoperator [31,32]

$$\mathcal{L}\hat{\rho} = -\sum_c \frac{\gamma_c}{2}(\hat{\rho}\hat{S}_c^+\hat{S}_c^- + \hat{S}_c^+\hat{S}_c^-\hat{\rho} - 2\hat{S}_c^-\hat{\rho}\hat{S}_c^+). \tag{13}$$

Here c enumerates the set of all possible spontaneous decay channels for the considered energy levels, γ_c are the spontaneous decay rates and $\hat{S}_c^\pm$ are the excitation or deexcitation operators. The actual simulations are performed in the interaction representation. We use the QUANTUMOPTICS.JL package [33] written in the JULIA language [34].

To model the gate described above, we consider the ion at $t = 0$ described by the normalized phonon-ion wave function

$$|\psi_{\text{init}}\rangle = (c_0 |0\rangle_q + c_1 |1\rangle_q) \otimes |0\rangle_{\text{vib}}, \tag{14}$$

where $|n\rangle_{\text{vib}}$ is the nth Fock state of the vibrational mode, $|0\rangle_q$ and $|1\rangle_q$ are the qubit states encoded in the $3D_{5/2}$, $m = -1/2$, and $4S_{1/2}$, $m = -1/2$ levels, respectively, and $c_0 = c_1 = 1/\sqrt{2}$. The initial density matrix is $\hat{\rho}_{\text{init}} = |\psi_{\text{init}}\rangle\langle\psi_{\text{init}}|$. Then, we calculate the evolution under 200 pairs of combs pulses with the model parameters of Table I for different ion equilibrium positions x_0.

For the final density matrix $\hat{\rho}_{\text{fin}}$ in the interaction representation, we calculate the phase difference θ acquired between the qubit levels with the expression

$$\theta = \text{Arg}(\langle\psi_0|\hat{\rho}_{\text{fin}}|\psi_1\rangle), \tag{15}$$

where $|\psi_\alpha\rangle = |\alpha\rangle_q \otimes |0\rangle_{\text{vib}}$. Also, we calculate the populations $\rho_{\gamma\gamma}$ of the nonqubit states.

The numerical results match with the theoretical predictions of Secs. III and IV. The acquired qubit phase coincides with Eqs. (8) and (9) with the discrepancy of $\sim 10^{-3}$ [see Fig. 3(a)], which we associate with the higher-order terms of the Magnus expansion. This discrepancy does not contribute to the gate error, as it indicates only the inaccuracy of the analytical expression for the phase (8) and can be avoided with the appropriate calibration of the combs power. The probability of the phonon excitation also matches with the prediction of Eq. (B5) [see Fig. 3(b)]. The excitation of the nonqubit electronic levels remains on the level of 10^{-6} in agreement with the estimates of Sec. IV.

VI. CONCLUSION

We suggest a method for single-qubit addressing in the trapped ion linear chains based on the quadratic Stark shift induced by two counter-propagating frequency combs. The implementation requires only global laser beams and is applicable for the ion chain of any length. To realize a single-qubit gate on a target qubit, one should adjust the time delay between the combs pulses so that the target ion lies in the overlap region between the pulses and apply the train of combs pulses and additional continuous-wave laser fields. We present the detailed calculation of the gate parameters for ^{40}Ca$^+$ ions and find that the single-qubit rotations can be implemented with the low infidelity ($\sim 5 \times 10^{-4}$) at moderate gate times (~ 8 μs). Also, our method can be extended for the isoelectronic ^{88}Sr$^+$, ^{138}Ba$^+$, and ^{226}Ra$^+$ ions by the appropriate choice of the setup parameters. We believe that our findings provide useful insight into quantum operations in trapped ion chains.

APPENDIX A: LEAKAGE TO THE NONQUBIT ION LEVELS

Here we analyze the leakage to the nonqubit ion levels. They can belong to either $S_{1/2}$, $D_{3/2}$, or $D_{5/2}$ manifolds. For the qubit state 0 belonging to the $D_{5/2}$ manifold, leakage is possible to the D sublevels, and for the qubit state 1 belonging to the $S_{1/2}$ manifold, the leakage is possible to the nonqubit $S_{1/2}$ component. For all listed pairs of electronic levels, transitions with the change of the vibrational state are also possible.

Assuming that the ion is in the qubit state α, we find the transition amplitude due to the action of the train of pulses to the nonqubit state γ. It can be approximated as the sum of transition amplitudes associated with the action of each couple of pulses. Each of these processes is a two-photon process corresponding to the absorption and emission of a photon, therefore, the amplitude by the kth pulse can be written as $a_k = a_0 e^{i(\epsilon_\gamma - \epsilon_\alpha)kT}$. Therefore, the total amplitude reads

$$|a_{\text{tot}}| = \left| \sum_{k=0}^{N_{\text{pulses}}-1} a_0 e^{i(\epsilon_\gamma - \epsilon_\alpha)kT} \right| < \frac{|a_0|}{|\sin[(\epsilon_\alpha - \epsilon_\gamma)T/2]|}. \tag{A1}$$

The dominant contribution to a_0 comes from the second order of the Magnus expansion. For the transitions not affecting the vibrational state, it is the same order as the phase shift per pulse. At the gate times and repetition rates that we consider $a_0 \sim \theta_{\text{gate}}/N_{\text{pulses}} \sim 10^{-3}$. For transitions changing both the electronic and the vibrational states, the amplitude is additionally multiplied by the Lamb-Dicke parameter $a_0 \propto \eta\theta_{\text{gate}}/N_{\text{pulses}}$. Given the Lamb-Dicke regime, we neglect the contribution of such transitions into error.

When the leakage occurs from the qubit state 0 to the nonqubit fine-structure $D_{3/2}$ sublevel, the transition frequency is $\epsilon_{D_{5/2}} - \epsilon_{D_{3/2}} = 2\pi \times 1.8287$ THz. Keeping the repetition rate ν_{rep} unequal to an integer fraction of $(\epsilon_{D_{5/2}} - \epsilon_{D_{3/2}})/(2\pi)$, one can easily ensure that $|\sin[(\epsilon_{D_{5/2}} - \epsilon_{D_{3/2}})T/2]| \sim 1$. For example, for the repetition rate of 100 MHz, the energy difference can be represented as $\epsilon_{D_{5/2}} - \epsilon_{D_{3/2}} = 2\pi(k + \Delta k)\nu_{\text{rep}}$, where $k = 18\,287$ and $\Delta k = 0.34$. At these conditions, the probability of the transition to the $D_{3/2}$ sublevels remains as small as $\sim \theta_{\text{gate}}^2/N_{\text{pulses}}^2 \sim 10^{-6}$.

For the case of the leakage from the qubit state to other Zeeman sublevels of the same manifold, the transition frequency equals the Zeeman splitting. Assuming the Zeeman splitting of $\nu_z = 2$ MHz and using Eq. (A1), we obtain the transition probability below $(\frac{\theta_{\text{gate}} \nu_{\text{rep}}}{2\pi N_{\text{pulses}} \nu_z})^2 \sim 10^{-4}$.

APPENDIX B: EXCITATION OF THE VIBRATIONAL LEVELS

The transitions between the vibrational levels can be taken into account in the following way. As femtosecond pulses are much faster than the periods of the ion motion, one can neglect the time dependence of the operator $\hat{x}$ for each pulse. This allows expressing the evolution operator of the kth pulse through the x-dependent evolution operator $U_k(x)$:

$$U_k = U_k[\hat{x}(t_k)]. \tag{B1}$$

As the evolution operator for each pulse is approximately diagonal, for two-qubit levels it takes the form

$$U_k = \begin{pmatrix} e^{i\delta\theta_0[\hat{x}(t_k)]} & 0 \\ 0 & e^{i\delta\theta_1[\hat{x}(t_k)]} \end{pmatrix}. \tag{B2}$$

The phases per pulse are small, therefore, we approximate the evolution of the wave function by a continuous function. Thus, the evolution can be described by the effective Hamiltonian

$$H_{\text{eff}} = \frac{1}{T} \begin{pmatrix} \delta\theta_0(\hat{x}) & 0 \\ 0 & \delta\theta_1(\hat{x}) \end{pmatrix}. \tag{B3}$$

In the Lamb-Dicke regime, the expansion of the phases in deviations from the equilibrium position reads

$$\delta\theta_\alpha(\hat{x}_i) = \delta\theta_\alpha(x_0) + \frac{1}{k_c} \frac{\partial \delta\theta_\alpha}{\partial x} \sum_\lambda \eta_{i\lambda}(a_\lambda + a_\lambda^\dagger). \tag{B4}$$

As the angles $\delta\theta_\alpha(x)$ depend only on the axial coordinate x, only axial modes contribute to the sum in Eq. (B4). Finally, the probability of phonon excitation (assuming that the gate acts on the ith ion being in the level α) can be easily calculated with the first-order perturbation theory

$$P_{i\alpha} = \frac{1}{k_c^2} \left(\frac{\partial \delta\theta_\alpha}{\partial x} \right)^2 \sum_\lambda \frac{|\eta_{i\lambda}|^2 |e^{i\omega_\lambda t_{\text{gate}}} - 1|^2}{\omega_\lambda^2 T^2}$$

$$< \frac{1}{k_c^2} \left(\frac{\partial \delta\theta_\alpha}{\partial x} \right)^2 \sum_\lambda \frac{4|\eta_{i\lambda}|^2}{\omega_\lambda^2 T^2}. \tag{B5}$$

One can see that the probability is proportional to $(\frac{\partial \delta\theta_\alpha}{\partial x})^2$. Therefore, it vanishes for the ion at the center of the pulses overlap region.

We estimate the phonon excitation probability for the ion slightly deviating from the center of the overlap region. For the gate angle of $\pi/2$ and the deviation from the pulse overlap region of 30 nm, we calculate the phonon excitation probability with Eq. (B5). We considered ion chains of different length N_{ions} and different gate times, including the case of a single ion with the parameters of Table I. For each $N_{\text{ions}} > 1$, we chose the axial frequency $\nu_{\text{ax}} = \omega_{\text{ax}}/(2\pi)$ small enough to ensure stability of the linear configuration at the radial frequency $\omega_{\text{rad}}/(2\pi) = 1$ MHz. The Lamb-Dicke parameters were found by diagonalization of the ions Hessian matrix as in [35] assuming harmonic potential in axial and radial directions. According to the dependencies shown in Fig. 4, even for chains with 20 ions with a low axial frequency of 110 kHz, the gate time can be chosen to so that the error remains on the level of 3×10^{-4}.

[1] A. Bermudez, X. Xu, R. Nigmatullin, J. O'Gorman, V. Negnevitsky, P. Schindler, T. Monz, U. G. Poschinger, C. Hempel, J. Home, F. Schmidt-Kaler, M. Biercuk, R. Blatt, S. Benjamin, and M. Müller, Phys. Rev. X **7**, 041061 (2017).

[2] C. D. Bruzewicz, J. Chiaverini, R. McConnell, and J. M. Sage, Appl. Phys. Rev. **6**, 021314 (2019).

[3] H. Häffner, F. Schmidt-Kaler, W. Hänsel, C. F. Roos, T. Körber, M. Chwalla, M. Riebe, J. Benhelm, U. D. Rapol, C. Becher, and R. Blatt, Appl. Phys. B **81**, 151 (2005).

[4] P. Wang, C.-Y. Luan, M. Qiao, M. Um, J. Zhang, Y. Wang, X. Yuan, M. Gu, J. Zhang, and K. Kim, Nat. Commun. **12**, 233 (2021).

[5] J. Benhelm, G. Kirchmair, C. F. Roos, and R. Blatt, Nat. Phys. **4**, 463 (2008).

[6] C. R. Clark, H. N. Tinkey, B. C. Sawyer, A. M. Meier, K. A. Burkhardt, C. M. Seck, C. M. Shappert, N. D. Guise, C. E. Volin, S. D. Fallek, H. T. Hayden, W. G. Rellergert, and K. R. Brown, Phys. Rev. Lett. **127**, 130505 (2021).

[7] I. Pogorelov, T. Feldker, C. D. Marciniak, L. Postler, G. Jacob, O. Krieglsteiner, V. Podlesnic, M. Meth, V. Negnevitsky, M. Stadler, B. Höfer, C. Wächter, K. Lakhmanskiy, R. Blatt, P. Schindler, and T. Monz, PRX Quantum **2**, 020343 (2021).

[8] S. Debnath, N. M. Linke, C. Figgatt, K. A. Landsman, K. Wright, and C. Monroe, Nature (London) **536**, 63 (2016).

[9] K. Wright, K. M. Beck, S. Debnath, J. M. Amini, Y. Nam, N. Grzesiak, J.-S. Chen, N. C. Pisenti, M. Chmielewski, C. Collins *et al.*, and Nat. Commun. **10**, 5464 (2019).

[10] P. Richerme, C. Senko, J. Smith, A. Lee, S. Korenblit, and C. Monroe, Phys. Rev. A **88**, 012334 (2013).

[11] J. Smith, A. Lee, P. Richerme, B. Neyenhuis, P. W. Hess, P. Hauke, M. Heyl, D. A. Huse, and C. Monroe, Nat. Phys. **12**, 907 (2016).

[12] J. Zhang, G. Pagano, P. W. Hess, A. Kyprianidis, P. Becker, H. Kaplan, A. V. Gorshkov, Z.-X. Gong, and C. Monroe, Nature (London) **551**, 601 (2017).

[13] C. Monroe, W. C. Campbell, L.-M. Duan, Z.-X. Gong, A. V. Gorshkov, P. W. Hess, R. Islam, K. Kim, N. M. Linke, G. Pagano, P. Richerme, C. Senko, and N. Y. Yao, Rev. Mod. Phys. **93**, 025001 (2021).

[14] C. Monroe and J. Kim, Science **339**, 1164 (2013).

[15] M. L. Day, K. Choonee, Z. Chaboyer, S. Gross, M. J. Withford, A. G. Sinclair, and G. D. Marshall, Quantum Sci. Technol. **6**, 024007 (2021).

[16] Y. Wang, S. Crain, C. Fang, B. Zhang, S. Huang, Q. Liang, P. H. Leung, K. R. Brown, and J. Kim, Phys. Rev. Lett. **125**, 150505 (2020).

[17] K. K. Mehta, C. D. Bruzewicz, R. McConnell, R. J. Ram, J. M. Sage, and J. Chiaverini, Nat. Nanotechnol. **11**, 1066 (2016).

[18] S. T. Cundiff and J. Ye, Rev. Mod. Phys. **75**, 325 (2003).

[19] D. Hayes, D. N. Matsukevich, P. Maunz, D. Hucul, Q. Quraishi, S. Olmschenk, W. Campbell, J. Mizrahi, C. Senko, and C. Monroe, Phys. Rev. Lett. **104**, 140501 (2010).

[20] W. C. Campbell, J. Mizrahi, Q. Quraishi, C. Senko, D. Hayes, D. Hucul, D. N. Matsukevich, P. Maunz, and C. Monroe, Phys. Rev. Lett. **105**, 090502 (2010).

[21] J. Mizrahi, C. Senko, B. Neyenhuis, K. G. Johnson, W. C. Campbell, C. W. S. Conover, and C. Monroe, Phys. Rev. Lett. **110**, 203001 (2013).

[22] S. H. Autler and C. H. Townes, Phys. Rev. **100**, 703 (1955).

[23] M. A. Nielsen and I. L. Chuang, *Quantum Computation and Quantum Information: 10th Anniversary Edition* (Cambridge University Press, Cambridge, England, 2010).

[24] J. Jiang, L. Jiang, Z. W. Wu, D.-H. Zhang, L.-Y. Xie, and C.-Z. Dong, Phys. Rev. A **99**, 032510 (2019).

[25] A. Kramida, Yu. Ralchenko, J. Reader, and NIST ASD Team, NIST Atomic Spectra Database (ver. 5.9), [Online]. Available: https://physics.nist.gov/asd [2022, May 20]. National Institute of Standards and Technology, Gaithersburg, MD. (2021).

[26] W. Magnus, Commun. Pure Appl. Math. **7**, 649 (1954).

[27] V. B. Berestetskii, L. P. Pitaevskii, and E. M. Lifshitz, *Quantum Electrodynamics* (Elsevier, Amsterdam, 2012).

[28] J. Thom, B. Yuen, G. Wilpers, E. Riis, and A. G. Sinclair, Appl. Phys. B **124**, 90 (2018).

[29] V. Gorini, A. Kossakowski, and E. C. G. Sudarshan, J. Math. Phys. **17**, 821 (1976).

[30] G. Lindblad, Commun. Math. Phys. **48**, 119 (1976).

[31] Z. Ficek and S. Swain, *Quantum Interference and Coherence* (Springer, New York, 2005).

[32] G. S. Agarwal, Quantum statistical theories of spontaneous emission and their relation to other approaches, *Quantum Optics*, edited by G. Höhler, Springer Tracts in Modern Physics, Vol. 70 (Springer, Berlin, Heidelberg, 1974).

[33] S. Krämer, D. Plankensteiner, L. Ostermann, and H. Ritsch, Comput. Phys. Commun. **227**, 109 (2018).

[34] J. Bezanson, A. Edelman, S. Karpinski, and V. B. Shah, SIAM Rev. **59**, 65 (2017).

[35] D. F. V. James, Appl. Phys. B **66**, 181 (1998).